Stochastic Dynamics of the Midlatitude Atmospheric Jet

BRIAN F. FARRELL

Department of Earth and Planetary Sciences, Harvard University, Cambridge, Massachusetts

PETROS J. IOANNOU

Center for Meteorology and Physical Oceanography, Massachusetts Institute of Technology, Cambridge, Massachusetts

ABSTRACT

The innate tendency of the background straining field of the midlatitude atmospheric jet to preferentially amplify a subset of disturbances produces a characteristic response to stochastic perturbation whether the perturbations are internally generated by nonlinear processes or externally imposed. This physical property of enhanced response to a subset of perturbations is expressed analytically through the nonnormality of the linearized dynamical operator, which can be studied to determine the transient growth of particular disturbances over time through solution of the initial value problem or, alternatively, to determine the stationary response to continual excitation through solution of the related stochastic problem. Making use of the fact that the background flow dominates the strain rate field, a theory for the turbulent state can be constructed based on the nonnormality of the dynamical operator linearized about the background flow. While the initial value problem provides an explanation for individual cyclogenesis events, solution of the stochastic problem provides a theory for the statistics of the ensemble of all cyclones including structure, frequency, intensity, and resulting fluxes of heat and momentum, which together constitute the synoptic-scale influence on midlatitude climate. Moreover, the observed climate can be identified with the background thermal and velocity structure that is in self-consistent equilibrium with both its own induced fluxes and the imposed large-scale thermal forcing. In order to approach the problem of determining the self-consistent statistical equilibrium of the midlatitude jet it is first necessary to solve the stochastic problem for the mixed baroclinic/barotropic jet because fluxes of both heat and momentum are involved in this balance.

In this work the response to stochastic forcing of a linearized nonseparable quasigeostrophic model of the midlatitude jet is solved. The observed distribution of transient eddy variance with frequency and wavenumber, the observed vertical structures, and the observed heat and momentum flux distributions are obtained. Associated energetics and implications for maintenance of the climatological jet are discussed.

1. Introduction

To a first order, the structure of the midlatitude jet is determined by adjustment to geostrophic balance between the thermal forcing produced by differential insolation between the equator and pole and the wave-induced fluxes of heat and momentum arising from synoptic-scale transient disturbances that are distributed stochastically in space and time.

Because of the central role of synoptic-scale eddies in midlatitude climate, obtaining a physically based theory for the statistical distribution of eddy variance and fluxes in the mixed baroclinic/barotropic midlatitude jet is central to a comprehensive understanding of the general circulation and the global climate system. One current theory for the production and maintenance of perturbation variance in baroclinic jets envisions that

the undisturbed background flow supports exponentially growing normal modes and that infinitesimal perturbations projecting on the unstable mode of maximum growth rate become exponentially dominant and ultimately mature into a wave of finite amplitude. When applied to the origin of cyclones this theory predicts that the wavelength and structure of the nascent cyclone will be that of the most rapidly growing modal instability and that the attendant fluxes will at least initially resemble those produced by this instability (Holton 1992; Pedlosky 1987). When applied to the problem of obtaining ensemble-mean quantities, modal instability theory has been interpreted to require wave-induced fluxes that are just sufficient to adjust the mean state to marginal stability (Stone 1978) or that the instability that best combines growth with effective exploitation of the available potential energy will control the heat flux (Held 1978). While modal instability theory has been applied successfully to simplified model problems, it has not produced an unambiguous correspondence with observations of either individual cyclogenesis events or of climatological-mean variance

Corresponding author address: Dr. Petros J. Ioannou, Center for Meteorology and Physical Oceanography, Massachusetts Institute of Technology, Building 54-1719, Cambridge, MA 02139.
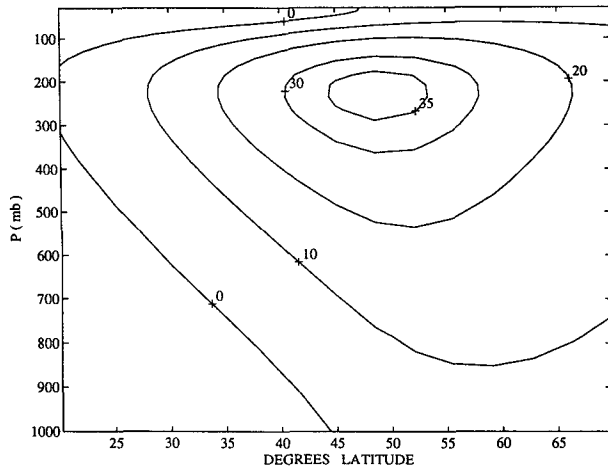
FIG. 1. The background zonal jet as a function of latitude and pressure. The functional form is given by Eq. (6) in which $U_0 = 40$ m s^{-1}, $A = 0.5$, and $C = 0.2$. Note that the meridional gradient is greatest on the equatorial side of the jet in accordance with observations (Trenberth 1992).

and fluxes as observed either in resolved models or the atmosphere (Petterssen 1955; Eliassen 1956; Salmon 1980; Stone et al. 1982; Vallis 1988).

An alternative theory envisions that maintenance of perturbation variance can be traced to amplification of nonmodal perturbations rather than to the growth of exponential modal instabilities (Farrell and Ioannou 1993a). In a forced/dissipative turbulent system with strong rates of strain but in which disruption due to wave–wave interaction prevents asymptotic dominance of the exponential modal instability from being established it is still possible for the flow to behave as an amplifier of the subspace of rapidly but transiently growing perturbations and for these growing perturbations to be continually replenished by nonlinear wave–wave interactions leading to maintenance of turbulent variance (Farrell and Ioannou 1993b, 1993c). In fact, disruption and scattering as parameterized in such a model constitute the entire essential role of nonlinearity in turbulence because the energetic exchange between the mean flow and the perturbations is fully accounted for by terms retained in the linearization (Joseph 1976).

A number of theoretical and observational advances (Farrell 1985, 1989; Sanders 1986; Nordeng 1990) support a generalized stability theory in which nonmodal growth mechanisms provide the explanation for the origin of synoptic-scale disturbances. Moreover, a theory based on the dynamics of nonnormal operators can also be applied to understanding the maintenance of the statistical climate (Farrell and Ioannou 1993c, 1994b). These previous reports developed the statistical calculus for nonnormal operators and applied it to a baroclinic jet without any barotropic shear. However, the important role of momentum flux in maintaining the jet requires that the statistical dynamics of a sto-

chastically forced nonseparable baroclinic/barotropic jet be examined in order to obtain consistent fluxes and tendencies.

2. Stochastic dynamics of a mixed baroclinic–barotropic jet

a. The evolution operator

Consider stochastic excitation of a zonal baroclinic jet. Harmonic geopotential height perturbations in a β-plane channel with zonal wavenumber k obey the linearized quasigeostrophic potential vorticity equation [for details refer to Farrell and Ioannou (1993c)]:

$$\frac{d\phi}{dt} = \mathcal{B}\phi, \tag{1}$$

where

$$\mathcal{B} = \frac{e^{z/2}}{\sqrt{\epsilon}} (\Delta^{-1}(-ikU - R)\Delta - ik\Delta^{-1}Q_y) \frac{\sqrt{\epsilon}}{e^{z/2}}, \tag{2}$$

with

$$\Delta = \frac{\partial^2}{\partial z^2} + \frac{1}{\epsilon} \frac{\partial^2}{\partial y^2} - \left(\frac{k^2}{\epsilon} + S^2 - \frac{dS}{dz}\right). \tag{3}$$

Here U is the mean zonal wind, ϵ the square ratio of the Coriolis parameter to the Brunt–Väisälä frequency, and R a linear potential vorticity damping coefficient, which will be a free parameter. The mean potential vorticity gradient is given by

$$Q_y = \frac{\beta}{\epsilon} - \frac{1}{\epsilon} \frac{\partial^2 U}{\partial y^2} + 2S \frac{\partial U}{\partial z} - \frac{\partial^2 U}{\partial z^2}, \tag{4}$$

and the stability parameter is defined as

$$S = -\frac{1}{2} \left(\frac{1}{\epsilon} \frac{d\epsilon}{dz} - 1\right). \tag{5}$$

The background zonal wind profile is taken to be

$$U/U_0 = U(z) \operatorname{sech}^2(Ay) + C \tanh(y), \tag{6}$$

with y scaled by the Rossby radius of deformation $L_d = NH/f_0$, in which N is the Brunt–Väisälä frequency, f_0 is the Coriolis parameter and in which the scale height is taken to be $H = 7.5$ km, by which z is also scaled. The scaling velocity is taken to be $U_0 = 40$ m s^{-1}, and the size of the jet is controlled by the parameter A, which is initially set equal to 0.5, while the asymmetry of the jet is controlled by the parameter C, which is taken equal to 0.2. The vertical jet structure is given by

$$U(z)/s = z - (z - z_0)H(z|z_0)$$

$$+ (z/2 - z_0)H(z|z_1), \tag{7}$$

in which the smooth ramp function $H(z|z_i) = 1 + \tanh((z - z_i)/d)$ is used. The jet maximum is placed at $z_0 = 1.5$, while at $z_1 = 3$ we place a transition to no

flow. The sharpness of the transitions are controlled by the parameter d, which is taken to be $d = 0.6$. The nondimensional shear parameter is taken to be $s = 0.6$. We have nondimensionalized time by L_d/U_0. The zonal jet that results is shown in Fig. 1.

The operator Δ^{-1} is rendered unique by incorporation of boundary conditions at the ground resulting from the vertical velocity produced by Ekman pumping associated with a coefficient of vertical diffusion ν, which will be taken to be 20 m^2/s^{-1}. The boundary condition at the top of the atmosphere is taken to be vanishing vertical velocity at four scale heights. The jet is confined to a channel and the meridional velocity is set to zero at the channel walls. The Brunt–Väisälä frequency is taken equal to $N = 0.014$ s^{-1} in the troposphere and two times this above the tropopause, which is placed at the jet maximum.

Finite differencing of (1) reduces the continuous dynamical system to a finite dimensional dynamical system.

b. Determining the optimal perturbations

In order to proceed it is necessary to have a means of measuring the absolute and relative magnitudes of perturbations. Perturbation energy given by

$$E^t = \phi^\dagger \mathcal{M} \phi \qquad (8a)$$

is taken as this perturbation measure. In (8a) $\phi^\dagger$ is the Hermitian transpose of ϕ, and the energy metric is defined, for a meridional grid of width δy and vertical grid of width δz, by

$$\mathcal{M} = \frac{\delta y \delta z}{4} (k^2 \mathcal{EP} + \mathcal{D}_y^\dagger \mathcal{PD}_y + \mathcal{D}_z^\dagger \mathcal{EPD}_z), \qquad (8b)$$

where $\mathcal{D}_z$ is the discretized $\partial/\partial z$ operator; $\mathcal{D}_y$ the discretized $\partial/\partial y$ operator; $\mathcal{P} = \text{diag}(\rho_i)$, where diag denotes the diagonal matrix generated by the vector (ρ_i) in which ρ_i is the mean density at the ith grid; and $\mathcal{E} = \text{diag}(\epsilon_i)$ is the stratification matrix (Farrell and Ioannou 1993c).

We transform (1) into generalized velocity variables $u = \mathcal{M}^{1/2}\phi$ so that the usual L_2 norm corresponds to the square root of the mean energy. Under this transformation a perturbation u_0 at $t = 0$ evolves to time t according to

$$u^t = e^{\mathcal{A}t}u_0, \qquad (9)$$

in which $e^{\mathcal{A}t}$ is called the propagator. The corresponding energy amplification is given by

$$E^t = \frac{u_0^\dagger e^{\mathcal{A}^\dagger t}e^{\mathcal{A}t}u_0}{u_0^\dagger u_0}, \qquad (10)$$

where $\mathcal{A} = \mathcal{M}^{1/2}\mathcal{B}\mathcal{M}^{-1/2}$.

The optimally growing perturbation over time interval t is identified with the eigenvector of $e^{\mathcal{A}^\dagger t}e^{\mathcal{A}t}$ corresponding to the largest eigenvalue (Farrell 1989) or, equivalently, to the singular vector corresponding to the maxi-

mum singular value of $e^{\mathcal{A}t}$. The energy amplification optimized over all initial perturbations is consequently given by $\|e^{\mathcal{A}t}\|_2^2$ and is called the optimal growth.

Due to the nonnormality of the evolution operator (i.e., $\mathcal{A}\mathcal{A}^\dagger \neq \mathcal{A}^\dagger\mathcal{A}$) the growth or decay of perturbation energy cannot in general be obtained as the sum of the growths of the isolated modes of the system, as would be the case for a normal system. Further, the optimal growth is necessarily larger than the growth attained by the perturbation associated with the maximally growing eigenvalue. The optimal growth for the midlatitude jet shown in Fig. 1 is shown in Fig. 2 for various global zonal wavenumbers K (the global wavenumbers are estimated for 45° latitude). The linear potential vorticity damping has been chosen to produce a 9 d e-folding, and the coefficient of eddy diffusion in the Ekman parameter is taken to be $\nu = 20$ m^2 s^{-1}. For these parameters the zonal jet is asymptotically stable. Despite the absence of normal-mode growth there is substantial transient growth with a global optimum energy amplification of 65-fold for $K = 6$ and $T = 12$ d.

Inspection of Fig. 2 reveals the initial growth as the slope of the growth curve at the origin (this growth rate at $t = 0$ is the numerical abscissa of $\mathcal{A}$ [i.e., the maximal eigenvalue of the Hermitian operator $(\mathcal{A} + \mathcal{A}^\dagger)/2$]. Note that the optimal initial growth at time $t = 0$ increases with wavenumber, suggesting that the dominant cyclone scale cannot be simply related to the initial growth of an unbiased spectrum of waves. These results agree with the observations that small-scale cyclones can be effectively formed by baroclinic energetics, although they also subsequently decay rapidly. It is remarkable that there is neither a short- nor a long-wave cutoff in the numerical abscissa and only a very weak scale selection attributable to variation with wavenumber in initial growth rate.

Because of computational limitations, convergence could not be tested by doubling resolution. Instead, test integrations with meridional grid numbers ranging from $n_y = 9$ to 17 and vertical grid numbers from $n_z = 20$ to 45 were used. The tests included both the convergence of the dispersion properties of the modes [which were compared to the calculations of Lin and Pierrehumbert (1988)] and calculation of the time optimals. We found that good results were obtained for $n_y = 11$ and $n_z = 40$. With this resolution the integration is converged for approximately 25 d, suggesting that large numerical models with at least this resolution can be accurately integrated for a month considering only their linear dynamics. (Of course, our model cannot provide direct guidance for resolution of nonlinear dynamics.)

c. Determining the stationary statistics

In generalized velocity variables the stochastically forced perturbation potential vorticity equation takes the form

$$\frac{du_i}{dt} = \mathcal{A}_{ij}u_j + \mathcal{F}_{ij}\xi_j, \qquad (11)$$
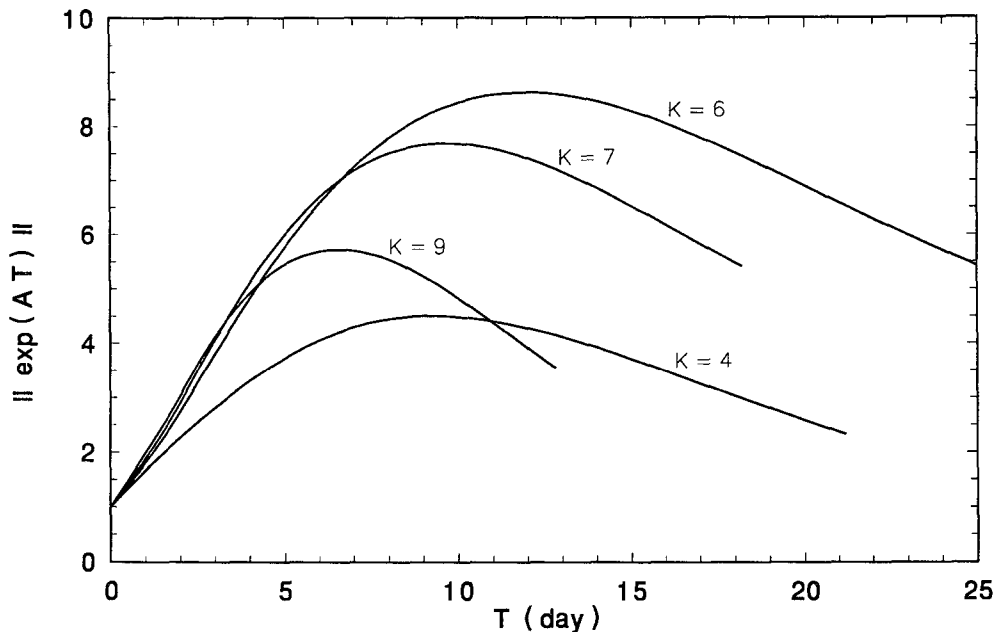
Asymmetric Jet, R = 9 d, ν = 20 m²/s

FIG. 2. The square root of the energy growth of the optimal perturbations as a function of the optimizing time T, in days for various zonal wavenumbers. This growth factor is given by the L_2 norm of $e^{\mathcal{A}T}$, where $\mathcal{A}$ is the evolution operator in generalized velocity coordinates. The background velocity is shown in Fig. 1 and the dissipation parameters are $1/R = 9$ days and $\nu = 20$ m² s⁻¹. Note that the flow is asymptotically stable. The global optimal occurs for $K = 6$ and an optimizing time $T \approx 12$ days for which a 65-fold energy amplification is achieved.

where ξ is the random forcing assumed to be a δ-correlated Gaussian white-noise process with zero mean and with unit variance

$$\langle \xi_i(t)\xi_j^*(t') \rangle = \delta_{ij}\delta(t - t'), \qquad (12)$$

where angle brackets denotes the ensemble average and the asterisk complex conjugation. Note that the stochastic forcing excites both independently and with unit magnitude each spatial forcing distribution as specified by the columns $f^{(j)}$ of the matrix $\mathscr{F}_{ij}$. We want to determine the evolution of the variance sustained by (11), which in physical variables is the ensemble-averaged energy $\langle E' \rangle = \langle u_i^*(t)u_i(t) \rangle$.

In this theory of the statistical steady state of the highly nonnormal baroclinic atmospheric jet the effects of nonlinearity are parameterized by white-noise forcing and a potential vorticity damping. In accord with the observation that the maintained variance in the atmosphere is finite we consider an asymptotically stable dynamical operator for which stationary statistics exist. For the jet in Fig. 1 and for Ekman damping consistent with a coefficient of vertical eddy momentum diffusion of $\nu = 20$ m² s⁻¹ the stability boundary is reached for a potential vorticity damping with an e-folding time of approximately 10 d. In most of our calculations we will assume a potential vorticity damping with e-folding time of 9 d, which is consistent with the observed de-

correlation time of disturbances at synoptic scale. This choice places the subcritical flow near neutrality as discussed in Farrell and Ioannou (1994b).

The random response u is linearly dependent on ξ and consequently is also Gaussian distributed. Therefore, the statistics of the response of the dynamical system are fully characterized by the first two moments. The first moment vanishes for large times if $\mathcal{A}$ is asymptotically stable. The expression for the second moment, the ensemble-average energy density, can be reduced to

$$\langle E' \rangle = \langle u(t)_i^* u(t)_i \rangle = \text{trace}(\mathscr{F}^\dagger \mathcal{K}'\mathscr{F}), \qquad (13)$$

where

$$\mathcal{K}' = \int_0^t e^{\mathcal{A}^\dagger(t-s)}e^{\mathcal{A}(t-s)}ds. \qquad (14)$$

The evolution equation for $\mathcal{K}'$ with initial condition $\mathcal{K}^0 = 0$ can be derived by direct differentiation of $\mathcal{K}'$. It is

$$\frac{d\mathcal{K}'}{dt} = \mathscr{I} + \mathcal{A}^\dagger \mathcal{K}' + \mathcal{K}'\mathcal{A}, \qquad (15)$$

in which $\mathscr{I}$ is the identity matrix. When the potential vorticity damping R is chosen so that $\mathcal{A}$ is asymptotically stable the stationary matrix $\mathcal{K}^\infty$ can be determined

by solving the asymptotic form of Eq. (15), which is the Liapunov equation:

$$\mathcal{A}^{\dagger}\mathcal{K}^{\infty} + \mathcal{K}^{\infty}\mathcal{A} = -\mathcal{I}. \tag{16}$$

Note that with an orthogonal set of forcing functions such that $\mathcal{F}\mathcal{F}^{\dagger} = \mathcal{I}$, the expression for the energy density simplifies to $\langle E^{\infty} \rangle = \text{trace}(\mathcal{K}^{\infty})$, and the variance is independent of the specific forcing distribution.

Second-order moments of all physical quantities can be deduced from the ensemble-average correlation matrix of the response $\mathcal{C}_{ij}^{t} = \langle u(t)_i u(t)_j^* \rangle$, which can be written using the propagator and forcing matrix associated with (11) as

$$\mathcal{C}^{t} = \int_{0}^{t} e^{\mathcal{A}(t-s)}\mathcal{F}\mathcal{F}^{\dagger}e^{\mathcal{A}^{\dagger}(t-s)}ds, \tag{17}$$

which assuming stationarity satisfies the Liapunov equation:

$$\mathcal{A}\mathcal{C}^{\infty} + \mathcal{C}^{\infty}\mathcal{A}^{\dagger} = -\mathcal{F}\mathcal{F}^{\dagger}. \tag{18}$$

Note that because $\mathcal{A}$ is nonnormal (i.e., $\mathcal{A}^{\dagger}\mathcal{A} \neq \mathcal{A}\mathcal{A}^{\dagger}$) the equation satisfied by the forcing correlation matrix (16) differs from that satisfied by the response correlation matrix (18).

Consider now the determination of an arbitrary second-order moment

$$S_{ij} = \langle (T_1\phi)_i (T_2^*\phi^*)_j \rangle, \tag{19}$$

where T_1 and T_2 are arbitrary operators. Because

$$\mathcal{C}_{ij}^{\phi} = \langle \phi_i \phi_j^* \rangle = (\mathcal{M}^{-1/2}\mathcal{C}^{\infty}\mathcal{M}^{-1/2})_{ij}, \tag{20}$$

we have that S is determined from the correlation matrix by

$$S = T_1 C^{\phi} T_2^{\dagger}. \tag{21}$$

d. Determining the EOFs and FOFs

Both $\mathcal{K}^{\infty}$ and $\mathcal{C}^{\infty}$ are by construction positive definite Hermitian forms with positive real eigenvalues associated with mutually orthogonal eigenvectors. Each eigenvalue of $\mathcal{C}^{\infty}$ equals the variance accounted for, under unbiased forcing, by the pattern of its corresponding eigenvector, and the pattern that corresponds to the largest eigenvalue contributes most to the variance. The eigenfunctions of $\mathcal{C}^{\infty}$ ordered by the magnitude of their eigenvalues are the structures that contribute most to the ensemble-average variance of the statistically steady state. These are the primary response structures (EOFs) of the dynamical system. The EOFs are interpreted dynamically by this stochastic theory, thus providing a link between observed atmospheric statistics and dynamical theory. On the other hand, eigenanalysis of $\mathcal{K}^{\infty}$ allows ordering of the forcing distributions according to their contribution to producing the variance of the statistically steady state and will be called FOFs [for further details see Farrell and Ioannou (1993b)].

If $\mathcal{A}$ is normal, as is the case in the absence of basic-state shear, $\mathcal{A}$, $\mathcal{C}'$, and $\mathcal{K}'$ commute, and the EOFs, FOFs, and the modes of the operator $\mathcal{A}$ coincide. For a normal $\mathcal{A}$ (18) can be immediately solved to yield for unitary forcing the steady-state ensemble-average energy:

$$\langle E^{\infty} \rangle = \text{trace}(\mathcal{C}^{\infty}) = \text{trace}(-(\mathcal{A} + \mathcal{A}^{\dagger})^{-1})$$

$$= \sum_{i} \frac{1}{2\,\text{Re}(-\lambda_i(\mathcal{A}))}, \tag{22}$$

where $\lambda_i(\mathcal{A})$ are the eigenvalues of $\mathcal{A}$. The variance maintained by normal dynamical operators has been extensively investigated in the past (cf. Wang and Uhlenbeck 1945). In normal systems the motion can be resolved into the orthogonal modes and the total variance found as the sum of contributions from the individual modes with this variance being inversely proportional to the modal damping rate. In such systems the forcing is the only energy source, and the maintained variance is simply accumulated from the forcing until modal damping produces an equilibrium.

For nonnormal dynamical operators the nonorthogonality of the modes allows the possibility of extraction of energy by the perturbations from the background flow field even in the absence of exponential instability. The energy balance in such a system is between the stochastic driving together with the induced extraction of energy from the background flow on the one hand and the dissipation on the other. This tapping of the energy of the mean flow can lead to levels of variance much greater than would be found in a normal system with the same modal dissipation rate. In fact, it can be shown that amplification of variance for unbiased forcing is a necessary consequence of the nonnormality of the evolution operator (Ioannou 1994).

The first EOF for the winter midlatitude jet is shown in Figs. 3a,b for $K = 6$. The first FOF for the same jet is shown in Figs. 4a,b for the same wavenumber. The least stable mode is shown in Figs. 5a,b. The impact of the nonnormality can be seen in these figures. Note here that because of the near neutrality of the atmosphere at $K = 6$ the first EOF is nearly identical to the least stable mode, and the first FOF is nearly identical to the adjoint of the least stable mode. A numerical model needs to resolve not only the energy-bearing scales of the EOFs but also the dynamically important FOFs, and these results indicate that this should be possible with resolution not greatly exceeding current GCM capabilities.

3. Wavenumber/frequency spectrum of the atmospheric jet

In order to determine the frequency response of our dynamical system we consider the Fourier transform of (11) to obtain an expression for the energy

$$\langle E^{\infty} \rangle = \frac{1}{2\pi} \int_{-\infty}^{\infty} F(\omega)d\omega \tag{23}$$
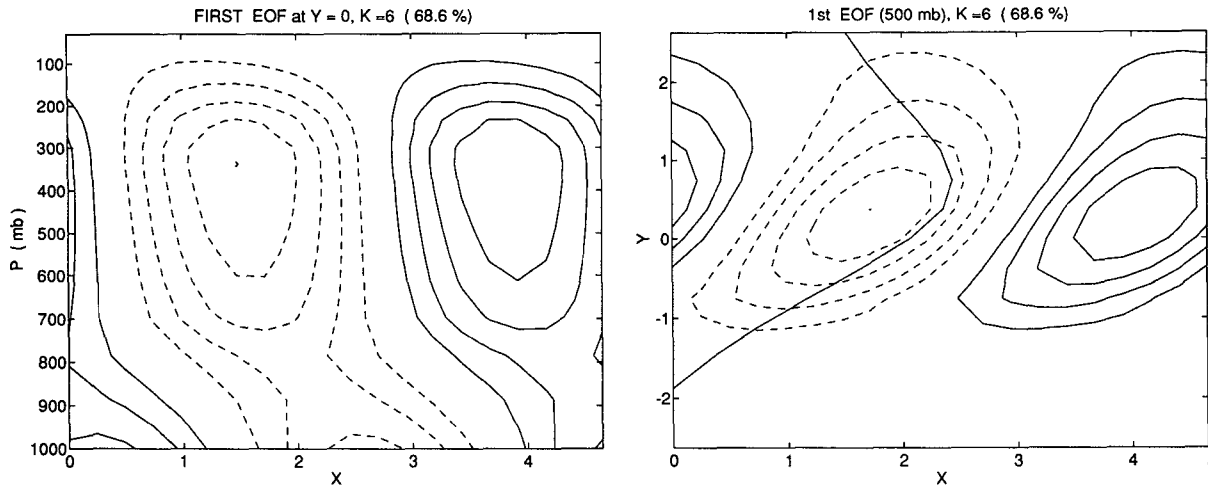
FIG. 3. Geopotential height distribution of the first EOF, accounting for 69% of the total eddy energy for $K = 6$. The background velocity is shown in Fig. 1 and the dissipation parameters are $1/R = 9$ days and $\nu = 20$ m^2 s^{-1}. (a) A zonal and pressure cross section at $Y = 0$. (b) A zonal and meridional cross section at 500 mb; the meridional structure of the mean wind at this height is marked for reference. Note that a unit length in Y corresponds to approximately 10 degrees of latitude.

as an integral over the frequency response

$$F(\omega) = \text{trace}(\mathcal{R}^\dagger(\omega)\mathcal{R}(\omega)), \qquad (24)$$

which is obtained making use of the resolvent

$$\mathcal{R}(\omega) = (i\omega\mathcal{I} - \mathcal{A})^{-1}. \qquad (25)$$

In other words, the power spectrum is given by the Frobenius norm of the resolvent $\mathcal{R}(\omega)$, which is equal to the square root of the sum of the squares of the singular values of the resolvent. In addition, the L_2 norm of $\mathcal{R}(\omega)$ gives the maximum response, which is produced by the optimal forcing structure at frequency ω. This maximum response is also equal to the maximum singular value of the resolvent.

When $\mathcal{A}$ is normal the response at any ω can be calculated knowing only the distance of the eigenspectrum from the forcing frequency ω. When $\mathcal{A}$ is nonnormal, the frequency response is by necessity underestimated by the proximity of ω to the eigenvalues of $\mathcal{A}$ (Farrell and Ioannou 1994a; Ioannou 1994). We will refer to the response calculated using only the eigenspectrum as the equivalent normal response. The frequency response and the equivalent normal response as a function of phase speed for $K = 6$ are shown in Fig. 6.

The spectrum of response to unbiased forcing as a function of period and zonal wavenumber is shown in Fig. 7. This graph reveals a pronounced response at low wavenumbers (4–6) with a period of around 10 days and at wavenumbers 7–8 and with a period of around 3 days. In contrast, the spectrum for the equivalent normal response (Fig. 8) does not exhibit this characteristic structure, which is in remarkable agreement with observations (Fraedrich and Böttger 1978; Schäfer 1979; Salby 1982; Randel and Stanford 1985; Randel and Held 1991).

This agreement with observations indicates that the atmospheric flow is subcritical but near neutrality. The magnitude of the peak depends primarily on the nonnormality of the operator, which increases as the neutral point is approached (cf. Figs. 7 and 8). As the flow is made more stable the peak in the spectrum at large scales is reduced. For an e-folding time of 5 d the spectra lose the observed structure and are characterized instead by a broad maximum at synoptic scales (cf. Farrell and Ioannou 1993c, 1994b). The sharp peak in the observed atmospheric spectra suggests that the equivalent potential vorticity damping places the flow near neutrality, and from this work it is clear that when the flow is close to neutral the shape of the resulting spectrum does not depend crucially on the details of the distribution of the noise so long as it is reasonably smooth. If instead of choosing a forcing that is white in energy we choose a forcing that is white in enstrophy, the spectrum will be multiplied by k^2. Because the spectrum is sharply peaked, such a modification affects mainly the shape of the background spectrum and does not change our qualitative conclusions. Our results demonstrate that the main determinant of the atmospheric spectra is the nonnormality of the near-neutral but subcritical atmospheric flow, which results from the linear advective operator, and that the structure of the noise and the effective damping rate are of relatively less importance.

The greatest response of the atmosphere to any unit norm forcing as a function of period and zonal wavenumber is shown in Fig. 9. This is obtained as the L_2 norm of the resolvent for each forcing period and wavenumber, and reveals the maximum possible response that can be obtained by the optimally configured forcing at this frequency and wavenumber. This maximum response and its associated forcing function can be ob-
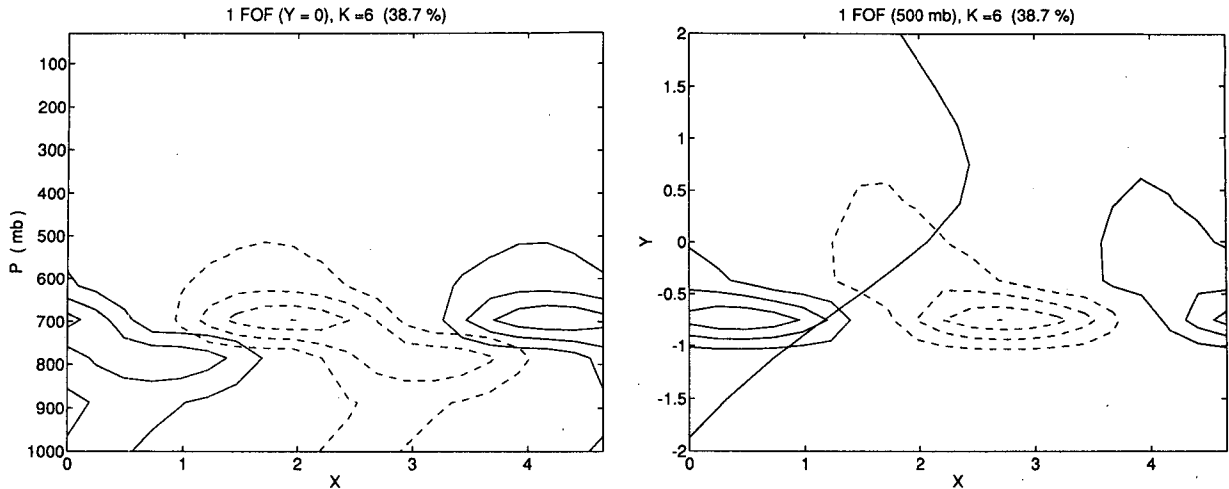
FIG. 4. Geopotential height distribution of the first FOF, which produces 39% of the total eddy energy for $K = 6$. The background velocity is shown in Fig. 1 and the dissipation parameters are $1/R = 9$ days and $\nu = 20$ m^2 s^{-1}. (a) A zonal and pressure cross section at $Y = 0$. (b) A zonal and meridional cross section at 500 mb; the meridional structure of the mean wind at this height is marked for reference. Note that a unit length in Y corresponds to approximately 10 degrees of latitude.

tained by singular value decomposition of (25) (only the optimal forcing is retained in Fig. 9, while all N members of the unbiased forcing set are retained in Fig. 7, accounting for the larger values in the latter figure).

4. Ensemble-average energy, heat, and momentum flux

The ensemble-average eddy energy density (m^2 s^{-2}) can be expressed in dimensional form for stochastic input E_{in} (W m^{-2}) as

$$\langle E \rangle = \frac{L_d}{U_0 H} \frac{E_{in}}{\rho_g N_f \delta y \delta z} \mathrm{diag}\left(\frac{\mathcal{C}^\infty}{\rho_i}\right), \quad (26)$$

where $\mathrm{diag}(\mathcal{C}^\infty/\rho_i)$ gives the diagonal elements of $\mathcal{C}^\infty$ divided by the corresponding value of the mean density normalized by its value at the ground ρ_g, and δy, δz are the grid intervals in the meridional and vertical direction (cf. Farrell and Ioannou 1994b). (The energy density was chosen because observational data are usually presented in this variable.) The number of degrees of freedom is N_f, which for N_f orthonormal forcings is also equal to trace ($\mathcal{FF}^\dagger$).

The vertical distribution of the ensemble-average heat flux can be expressed in dimensional form:

$$\langle H \rangle = c_p \langle \rho \overline{v\theta} \rangle = \frac{c_p T_g L_d}{gH} E_{in} \frac{\mathrm{diag}(\mathcal{H}^\infty)}{N_f}, \quad (27)$$

where $\mathrm{diag}(A)$ gives the diagonal elements of the matrix A, the bar denotes a phase average, T_g is a representative surface temperature, and c_p is the specific heat per unit mass. The heat flux matrix is

$$\mathcal{H}^\infty = \frac{k}{2} \mathrm{Im}(\mathcal{P}^{1/2} \mathcal{D}_z \mathcal{M}^{-1/2} \mathcal{C}^\infty \mathcal{M}^{-1/2} \mathcal{P}^{1/2}), \quad (28)$$

with the same notation as in (9). Note that knowledge of the correlation matrix is in general sufficient for determining any second-order moment.

The momentum flux can be expressed in dimensional form as

$$\langle M \rangle = \langle \rho \overline{uv} \rangle = \frac{L_d}{U_0 H} E_{in} \frac{\mathrm{diag}(\mathcal{M}^\infty)}{N_f}, \quad (29)$$

with

$$\mathcal{M}^\infty = -\frac{k}{2} \mathrm{Im}(\mathcal{P}^{1/2} \mathcal{D}_y \mathcal{M}^{-1/2} \mathcal{C}^\infty \mathcal{M}^{-1/2} \mathcal{P}^{1/2}). \quad (30)$$

Variation of the vertically averaged energy, heat flux, and momentum flux with wavenumber at the latitude of the jet maximum is shown in Fig. 10. Note that most of the transport is produced by global wavenumber 6 in agreement with results of an 8-year compilation of European Centre for Medium-Range Weather Forecasts (ECMWF) data (Randel and Held 1991). We might have expected the cyclone scales ($K > 9$) to dominate the eddy transport, but instead the picture that emerges is of the cyclones stochastically forcing the large-scale transient waves, which in turn produce most of the eddy transport. We note that this interpretation resembles that advanced by Palmén and Newton (1969) for maintenance of the observed large-scale transient waves in midlatitudes. In the theory described above, the prominence of the $K = 6$ scale results both from the nonnormality of the evolution operator and its near neutrality, which in turn results in part from the fact that Ekman damping is less effective at lower wavenumbers. The location of the wavenumber of maximum variance and heat and momentum transport indicates that the magnitude of mean effective Ekman parameter corresponds to a vertical diffusion coeffi-
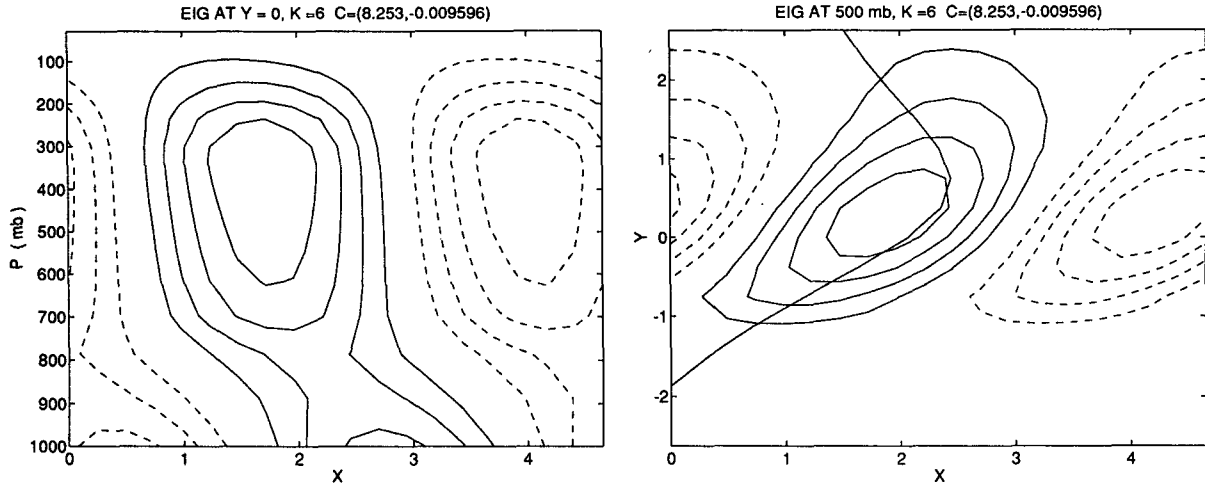
EIG AT Y = 0, K =6 C=(8.253,-0.009596)   EIG AT 500 mb, K =6 C=(8.253,-0.009596)

FIG. 5. Geopotential height distribution of the least damped mode for $K = 6$, which has a phase speed $C_r = 8.2$ m s^{-1} and a decay e-folding time of 100 days. The background velocity is shown in Fig. 1 and the dissipation parameters are $1/R = 9$ days and $\nu = 20$ m^2 s^{-1}. (a) A zonal and pressure cross section at $Y = 0$. (b) A zonal and meridional cross section at 500 mb; the meridional structure of the mean wind at this height is marked for reference (unit length in Y corresponds to approximately 10 degrees of latitude).

cient of 20–30 m^2 s^{-1}, a value that is consistent with the observed mean stress at the ground (Gill 1982; p. 332).

Analysis of ECMWF seasonal flux statistics performed by Randel and Held (1991) and independently by Amy Solomon at MIT (1994, unpublished manuscript; cf. Farrell and Ioannou 1994b) shows that this wavenumber 6 prominence is observed in both hemispheres during both the winter and summer months. A major simplification of climate dynamics is achieved if the midlatitude general circulation can be accurately described as a stochastic equilibrium between the mean thermal forcing and the Eliassen–Palm (EP) fluxes primarily arising from a single dominant wavenumber.

Normalized distributions in the vertical, at the latitude of the jet maximum, of the ensemble-average energy and heat flux per unit mass as a function of zonal wavenumber are shown in Fig. 11 and Fig. 12. (It should be noted that these calculations are strictly valid above the Ekman layer, which has been arbitrarily placed at 1000 mb in our calculations, instead of at ≈900 mb. This should be taken into consideration when comparing these vertical distributions of eddy statistics with observations.) The ensemble energy includes both kinetic and potential forms. The prominence at the ground is mainly due to potential energy as can be seen in a plot of the associated rms temperature fluctuation shown in Fig. 13. The corresponding distribution of the rms zonal eddy velocity and meridional eddy velocity is shown in Fig. 14 and Fig. 15, respectively. Examples of the meridional and vertical structure of the heat and momentum flux for wavenumbers 5 and 6 are shown in Figs. 16a,b and Figs. 17a,b. The derived distributions are in good agreement with the observed statistical distributions of these quantities (cf. Schubert et al. 1990; Trenberth 1992).

5. Momentum flux distributions

Held (1975) and Held and Andrews (1983) argued that the meridional extent of the jet controls the direction of the wave-induced momentum fluxes: jets that are broad relative to the Rossby radius of deformation and in which the baroclinic shear is comparable to that observed in midlatitude jets are associated with wave-induced upgradient momentum fluxes that tend to reinforce the westerly jet, while sufficiently narrowly confined jets lead to downgradient momentum fluxes and a tendency to decelerate the jet. It has been further argued that the size of the jet is determined by an equilibration associated with this mechanism. Held and Andrews (1983), extending the perturbation procedure of McIntyre (1970), showed that this intensification of broad jets and reduction of sharp jets is quite general. In their analysis the direction of the momentum fluxes depended both on the zonal scale of the fastest-growing mode in relation to the deformation radius and on the size of the jet scaled by the deformation radius. In contrast to these previous studies, which pivoted on modal instability, in this work the direction of the stochastically induced statistical equilibrium momentum fluxes is examined.

Referring to our parameterization of an asymmetric jet (6), the scale of the meridional variation of the jet L, in units of the Rossby radius L_d, is $L = 1/A$ (the half-width of the jet is approximately $2/A$). The mean flow tendency for a symmetric jet ($C = 0$) as a function of zonal wavenumber and meridional scale of the jet A is shown in Fig. 18. The corresponding mean flow tendency for an asymmetric jet ($C = 0.2$) is shown in Fig. 19. It can be seen that the momentum flux divergence changes sign as the size of the jet decreases: when the jet is broad ($A \leq 0.8 - 1$) the fluxes are upgradient,
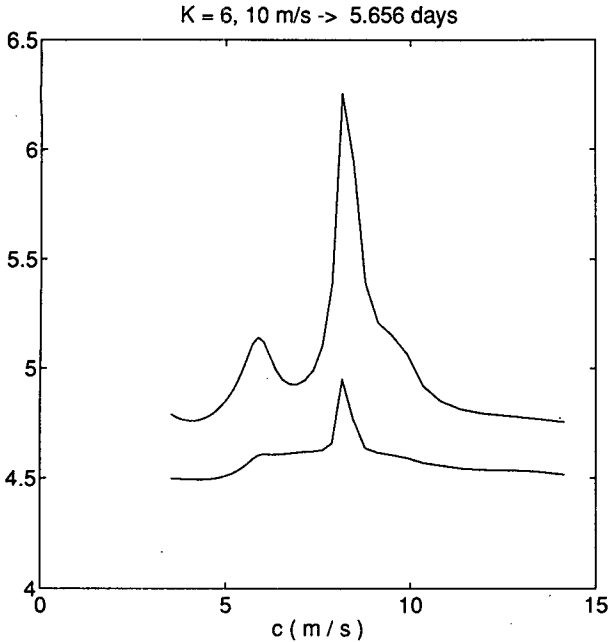
K = 6, 10 m/s -> 5.656 days

FIG. 6. The energy response (in a base 10 logarithmic plot) of the background flow to unbiased forcing as a function of phase speed. The lower curve gives the equivalent normal response in which the non-orthogonality of the modes is not taken into account. The background velocity is shown in Fig. 1 and the dissipation parameters are $1/R = 9$ days and $\nu = 20$ m^2 s^{-1}. The zonal wavenumber is $K = 6$, for which a phase speed of 10 m s^{-1} corresponds to a period of 5.6 d. The primary peak is at a period of 7 d, and the secondary peak, not captured by the equivalent normal response, is at a period of 9.5 d.

EQ. NORMAL STOCHASTIC log10 (F), R = 9 , nu = 20
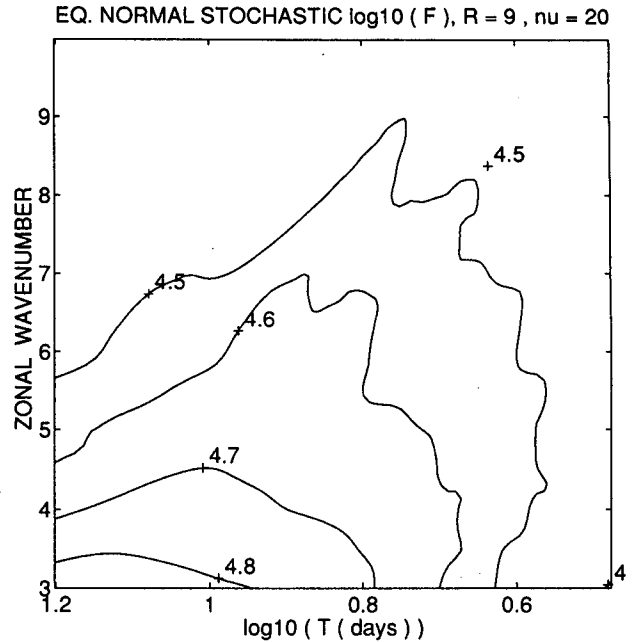
FIG. 8. The equivalent normal response variance as a function of period and zonal wavenumber. The vertical diffusion coefficient has been chosen to be $\nu = 20$ m^2 s^{-1}, and the e-folding time for the linear damping has been chosen to be 9 days. The equivalent normal response is derived by considering the response of the diagonalized linear operator.

STOCHASTIC log10 (F), R = 9 , nu = 20
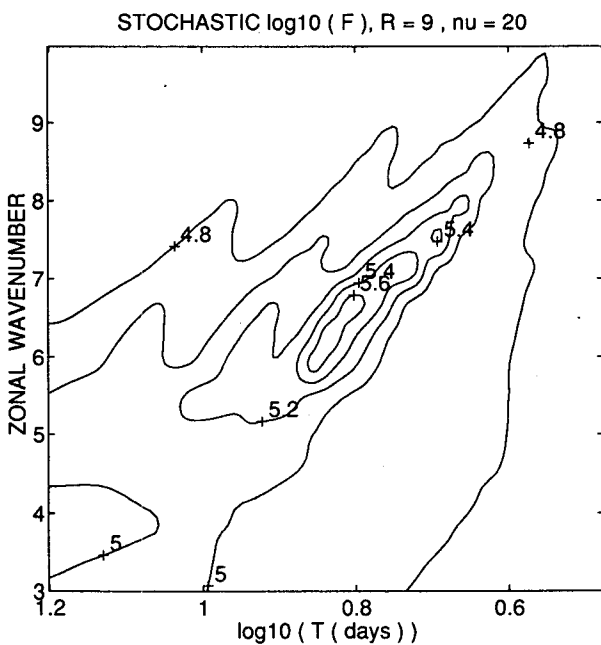
FIG. 7. The variance as a function of period and zonal wavenumber at 45° latitude. The vertical diffusion coefficient has been chosen to be $\nu = 20$ m^2 s^{-1}, and the e-folding time for the linear damping is 9 days.

log10 (II F II), R = 9 , nu = 20
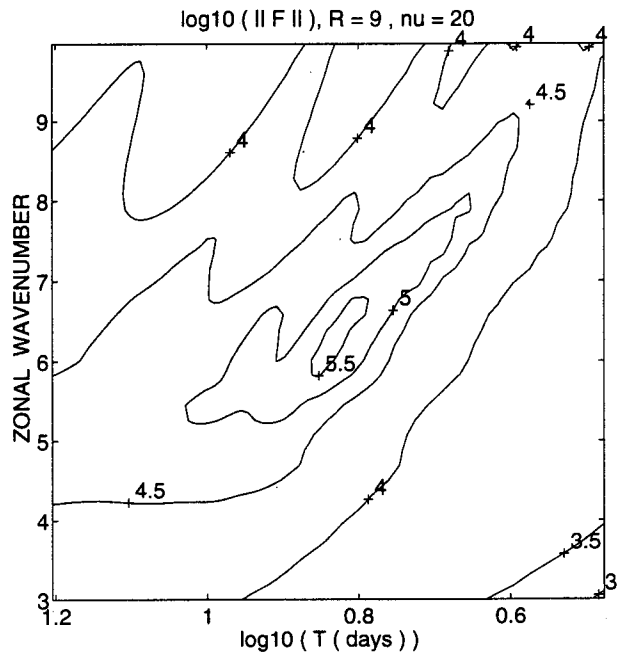
FIG. 9. The optimal energy response as a function of period and zonal wavenumber. The vertical diffusion coefficient has been chosen to be $\nu = 20$ m^2 s^{-1}, and the e-folding time for the linear damping is 9 days. Unit norm driving has been restricted to the optimal.
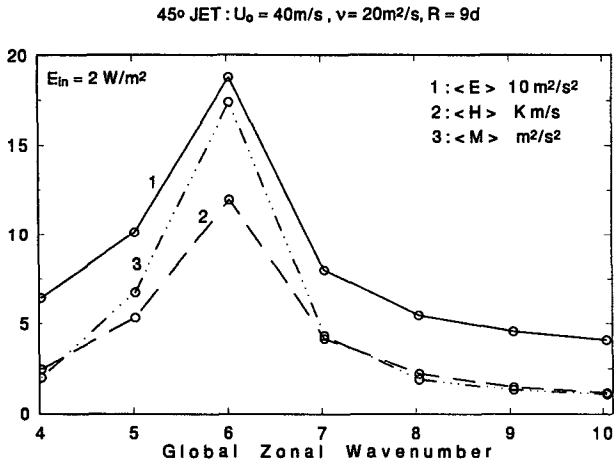
45° JET : U₀ = 40m/s , v= 20m²/s, R = 9d

FIG. 10. Variation of the vertically averaged ensemble-average energy $\langle E \rangle$ (solid line), transient heat flux $\langle H \rangle$ (dash line), and transient momentum flux $\langle M \rangle$ (dot–dash line) at the latitude of the jet maximum as a function of the zonal wavenumber. The stochastic driving is 2 W m^{-2}. The background velocity is shown in Fig. 1 and the dissipation parameters are $1/R = 9$ days and $\nu = 20$ m^2 s^{-1}.

and when the jet is narrow ($A \geq 0.8 - 1$) the fluxes are downgradient, in qualitative agreement with predictions from modal theory.

The observed winter jet corresponds approximately to $A = 0.5$. The latitudinal distributions of vertically averaged energy, heat flux, momentum flux, and momentum flux divergence for the dominant $K = 6$ wave are shown in Fig. 20a and Fig. 21a for $A = 0.5$ and $E_{in} = 1$ W m^{-2}. To attain the sea-

sonal-averaged eddy fluxes a stochastic input of the order of 3 W m^{-2} is required, which implies a maximum upgradient momentum flux divergence of ≈ 1 m s^{-1} day^{-1}. Note that in the absence of dissipation and because the vertically averaged contribution from induced mean meridional circulations vanishes due to continuity, the vertically averaged momentum flux divergence yields the vertically averaged mean flow acceleration (cf. Ioannou and Lindzen 1986). In the presence of friction, a stationary jet must be maintained against frictional deceleration by upgradient eddy momentum flux divergence. The average frictional retardation has been estimated to give a mean stress at the ground of $\approx 1/10$ N m^{-2} (Palmén and Newton 1969), and this leads to a deceleration of the atmospheric column of ≈ 0.83 m s^{-1} day^{-1}. It follows that our chosen atmospheric jet is in approximate stochastic equilibrium. Note also from Fig. 19 that for all $K < 10$ the momentum flux divergence is upgradient, consistent with observations.

The corresponding latitudinal distributions of vertically averaged energy, heat flux, momentum flux, and momentum flux divergence for the dominant $K = 6$ wave but for a narrow jet for $A = 1.2$ are shown in Fig. 20b and Fig. 21b. Here note that the eddy momentum flux divergence is downgradient, in contrast with observations.

6. Conclusions

Stochastic dynamics of a nonnormal system associated with a nonseparable baroclinic/barotropic midlatitude jet was examined in this work. When the jet is

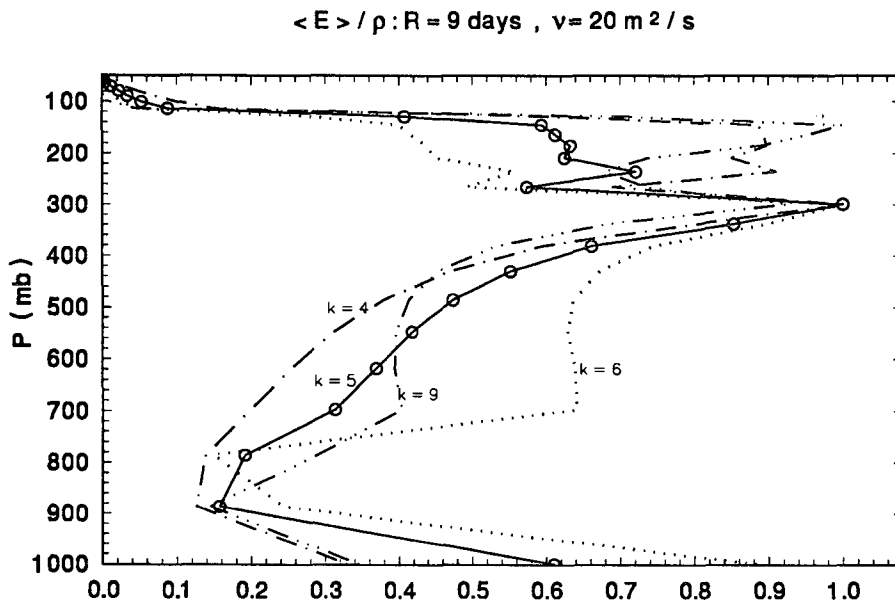$\langle E \rangle / \rho : R = 9$ days , $v = 20$ m² / s

FIG. 11. The normalized distribution of the ensemble-average energy for various global zonal wavenumbers as a function of pressure. The dissipation parameters are taken to be $\nu = 20$ m^2 s^{-1} and $1/R = 9$ days.
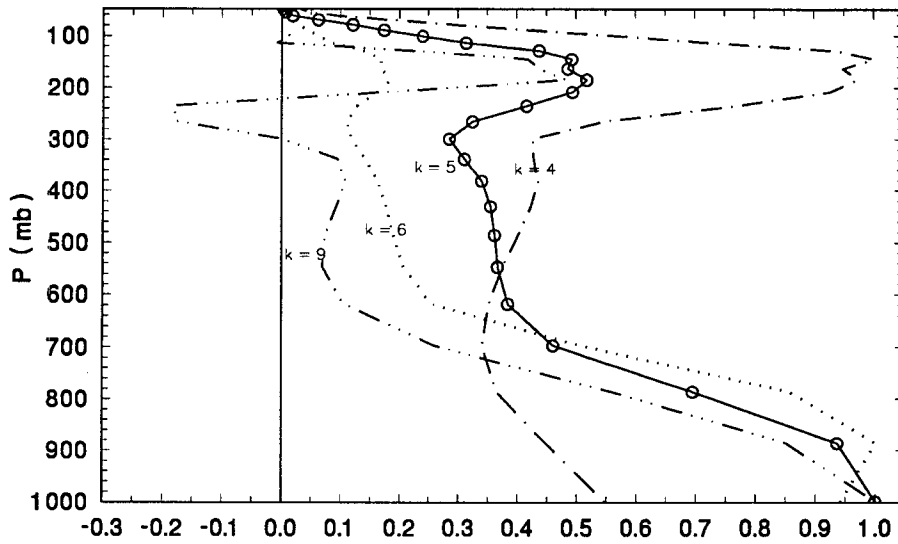
FIG. 12. The normalized distribution of the ensemble-average heat flux for various global zonal wavenumbers as a function of pressure. The dissipation parameters are taken to be $\nu = 20$ m^2 s^{-1} and $1/R = 9$ days.

forced stochastically and the response transformed to generalized velocity variables, the structures of the preferred response are found from eigenanalysis of the correlation matrix, which is in turn found as the solution of Liapunov equation (18). Moreover, the distinct set of forcing functions that contribute most to producing the variance are found by eigenanalysis of the forcing correlation matrix, which is in turn found as the solution of the related Liapunov equation (16). The forcing functions, the response functions, and the normal modes are distinct for nonnormal dynamical systems such as that associated with the jet studied here,
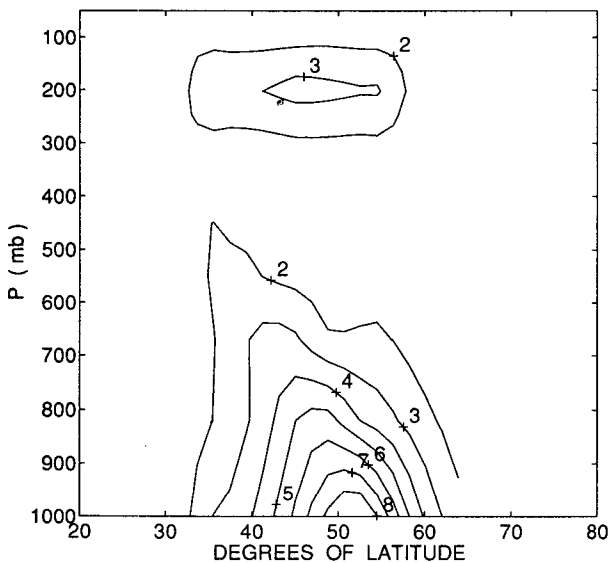
FIG. 13. The distribution with height and latitude of the rms temperature perturbation T in K for global zonal wavenumber 6. The dissipation parameters are taken to be $\nu = 20$ m^2 s^{-1} and $1/R = 9$ days. The stochastic forcing is $E_{in} = 1$ W m^{-2}.
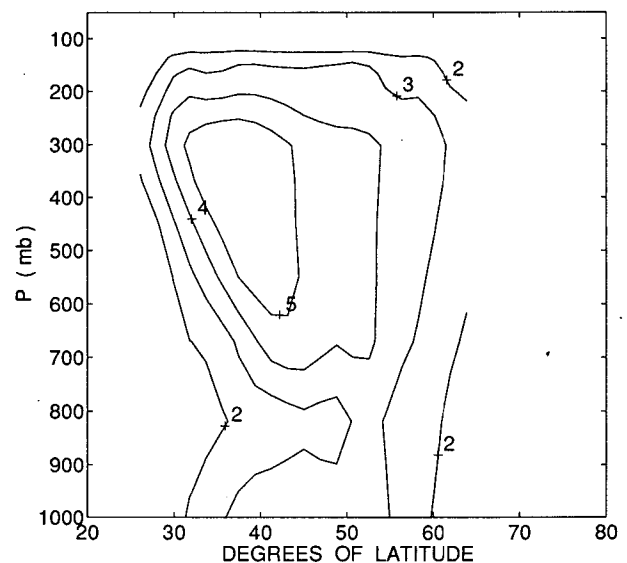

FIG. 14. The distribution with height and latitude of the rms eddy zonal velocity u in m s^{-1} for global zonal wavenumber 6. The dissipation parameters are taken to be $\nu = 20$ m^2 s^{-1} and $1/R = 9$ days. The stochastic forcing is $E_{in} = 1$ W m^{-2}.

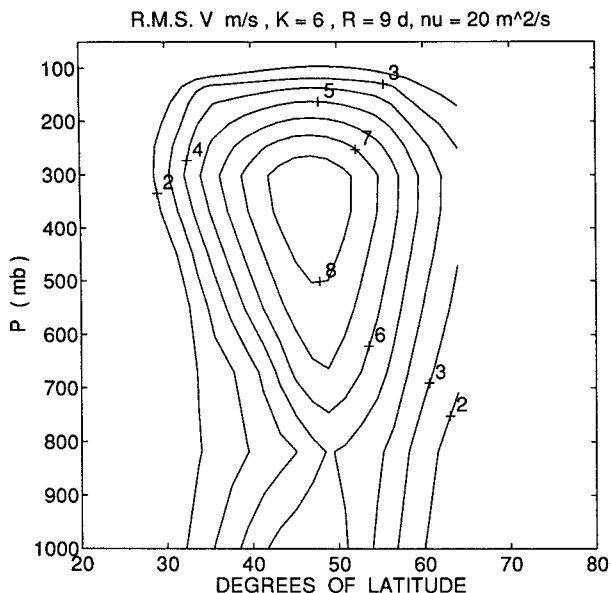R.M.S. V m/s , K = 6 , R = 9 d, nu = 20 m^2/s

FIG. 15. The distribution with height and latitude of the rms eddy meridional velocity v in m s^{-1} for global zonal wavenumber 6. The dissipation parameters are taken to be $\nu = 20$ m^2 s^{-1} and $1/R = 9$ days. The stochastic forcing is $E_{in} = 1$ W m^{-2}.

although these three are identical in the case of a normal system.

The variance produced by the preferred responses is found to have a wavenumber/frequency distribution in remarkable agreement with observations. In particular, the commonly observed wavenumber 6 response is obtained as well as the cyclone-scale response at higher frequency. The vertical/meridional structures associated with these waves are realistic and in particular display the secondary upper-level maximum seen in observations. The forcing functions reveal that the structures of the disturbances that contribute most to maintaining the variance are of higher vertical wavenumber but are not so highly structured as to pose insurmountable resolution requirements on numerical models. For the meridional scale of the observed mid-latitude jet, the heat flux is found to be concentrated near the ground and the momentum flux to be upgradient as observed.

The observed midlatitude jet was found to have a meridional scale for which the stochastic momentum flux is upgradient, in agreement with observations. It is to be expected that sufficiently sharp jets produce downgradient fluxes, and this was found to be so for jets with a half-width of approximately one Rossby radius.

The combined heat and momentum flux produced by stochastic forcing gives rise to momentum flux distributions the divergence of which reveals the expected tendency toward acceleration of the upper-level jet.

These distributions of variance and flux could be ascertained from solution of the linear stochastic equations, but, in addition to distributions, an amplitude of forcing is required in order to make quantitative application of the theory. This amplitude was determined by requiring that the stochastic solution yield the observed total variance. This level of forcing also produced heat and momentum fluxes that agree well with observations and, in particular, momentum flux divergence in quantitative agreement with observed surface stress.

As with any physical theory, the purpose of stochastic dynamics is both conceptual and practical. Conceptually, the theory provides a unifying mechanistic understanding of the turbulent atmosphere in terms of amplification of a subset of perturbations, the existence of
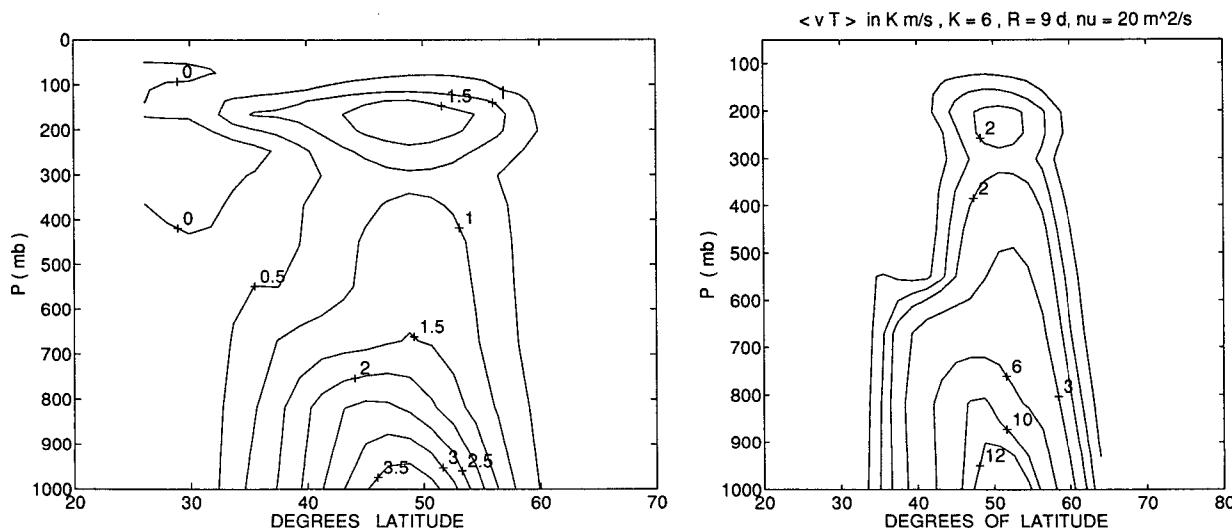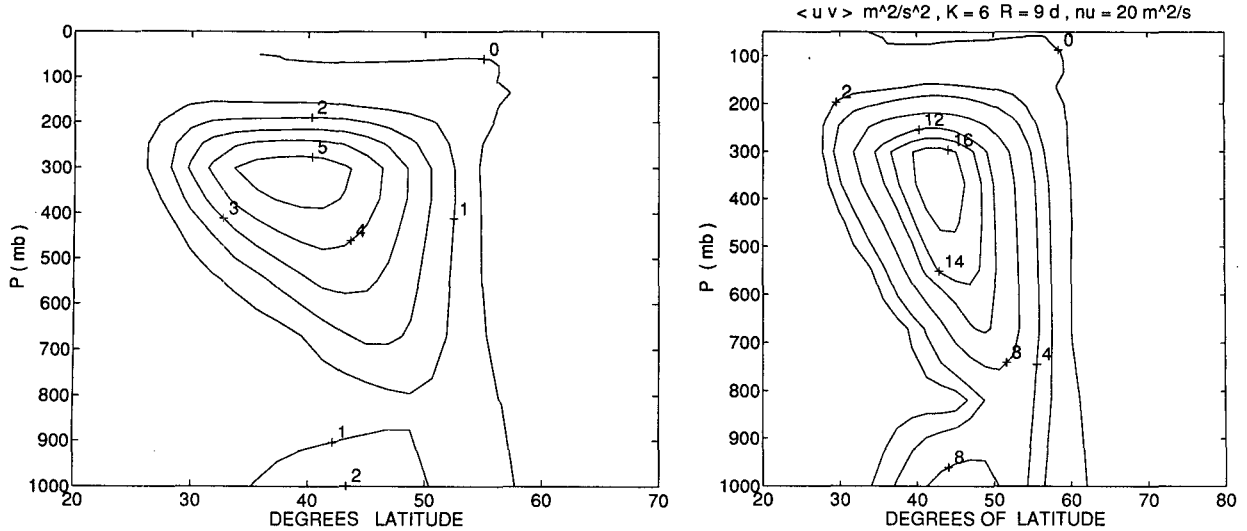

FIG. 16. The distribution with pressure and latitude of the ensemble-average heat flux: (a) for global zonal wavenumber 5; (b) for global zonal wavenumber 6. The dissipation parameters are taken to be $\nu = 20$ m^2 s^{-1} and $1/R = 9$ days. The stochastic forcing is $E_{in} = 1$ W m^{-2}.

FIG. 17. The distribution with pressure and latitude of the ensemble-average momentum flux: (a) for global zonal wavenumber 5; (b) for global zonal wavenumber 6. The dissipation parameters are taken to be $\nu = 20$ m^2 s^{-1} and $1/R = 9$ days. The stochastic forcing is $E_{in} = 1$ W m^{-2}.

which can be traced to the nonnormality of the underlying linear dynamics with the role of nonlinearity confined to providing the requisite scattering of perturbations into the growing subset so that a steady state can be obtained and augmenting the dissipation to account for disruption of the growing waves. This conceptual view directs attention to the nonnormality of the underlying dynamics and the distinct forcing and response functions arising from this nonnormality. In addition, the role of nonlinearity is reinterpreted from being the primary agent of the turbulence through its spectral interactions to playing a relatively minor, albeit vital, role
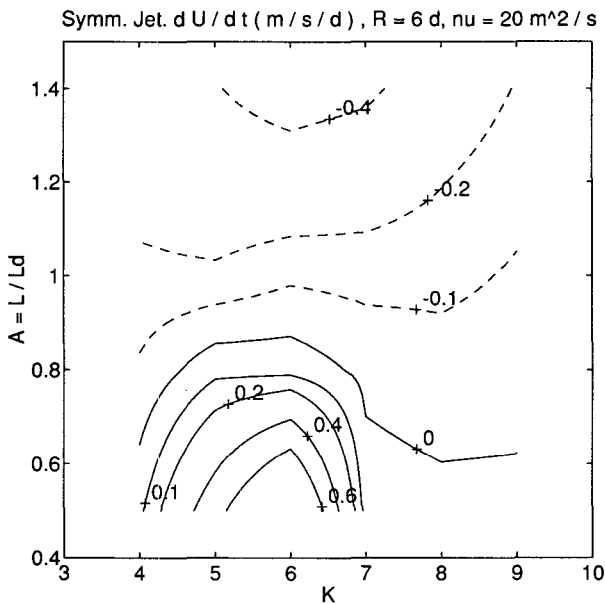

FIG. 18. The vertically averaged eddy momentum flux divergence in m s^{-1} day^{-1} at $Y = 0$ for a symmetric jet as a function of zonal wavenumber K and jet width A. The dissipation parameters are taken to be $\nu = 20$ m^2 s^{-1} and $1/R = 9$ days, and the stochastic forcing is $E_{in} = 1$ W m^{-2}. The observed winter midlatitude jet has $A \approx 0.5$. Positive values correspond to an accelerative tendency of the background flow at the jet maximum.
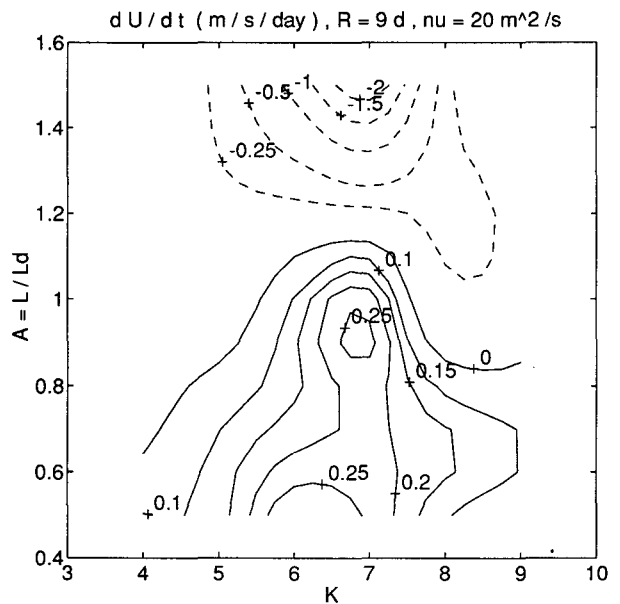
FIG. 19. The maximum vertically averaged eddy momentum flux divergence nearest to jet maximum in m s^{-1} day^{-1} for an asymmetric jet as a function of zonal wavenumber K and jet width A. The dissipation parameters are taken to be $\nu = 20$ m^2 s^{-1} and $1/R = 9$ days, and the stochastic forcing is $E_{in} = 1$ W m^{-2}. Positive values correspond to an accelerative tendency of the background flow near the jet maximum.
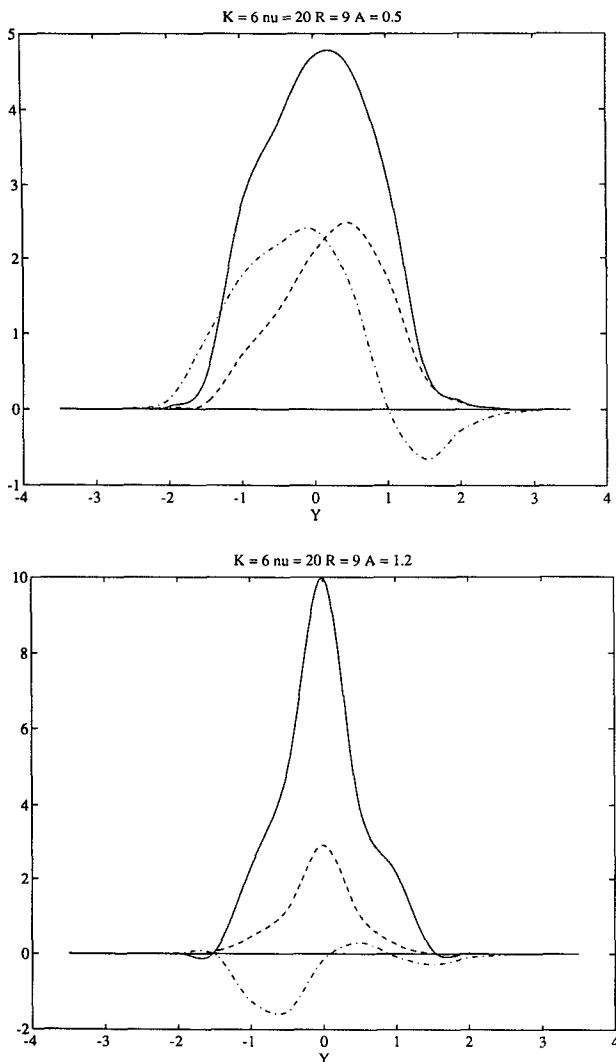
FIG. 20. Vertically averaged energy per unit mass (continuous curve) in units of $10 \, m^2 \, s^{-2}$, vertically averaged heat flux (dash curve) in $K \, m \, s^{-1}$, and momentum flux (dash–dot curve) in $m^2 \, s^{-2}$ function of latitude: (a) for $A = 0.5$; (b) for $A = 1.2$. The dissipation parameters are taken to be $\nu = 20 \, m^2 \, s^{-1}$ and $1/R = 9$ days, and the stochastic forcing is $E_{in} = 1 \, W \, m^{-2}$. Note that a unit in the abscissa corresponds to approximately 10 degrees of latitude.

in resupplying the growing subset as these are depleted through their transient nonmodal growth.

This mechanistic theory of quasigeostrophic turbulence in the highly baroclinic midlatitude jet exploits in an essential way the dominance of the mean flow as a source of energy maintaining the perturbation variance. Because the energetic exchange between the mean flow and the perturbations is imbedded in the dynamical operator linearized about the mean flow, this theory enjoys a simplification not shared by similar theories of turbulence in normal systems such as homogeneous isotropic turbulence. Without the simplification resulting from dominance of the nonnormal linear operator theories such as direct interaction approxi-

mation, random coupling model, test field model (cf. Lesieur 1993) require intricate specification of forcing and damping as a function of wavenumber. By contrast, in highly nonnormal systems such as the midlatitude jet the role of nonlinearity, while essential, is much more easily parameterized because the nonnormal operator dominates the response. This dominance of the nonnormality can be seen clearly in the examples comparing the nonnormal with the equivalent normal spectra. The predominance of wavenumber 5–6 in the variance and fluxes proceeds from the preferred response of the nonnormal dynamics at this wavenumber rather
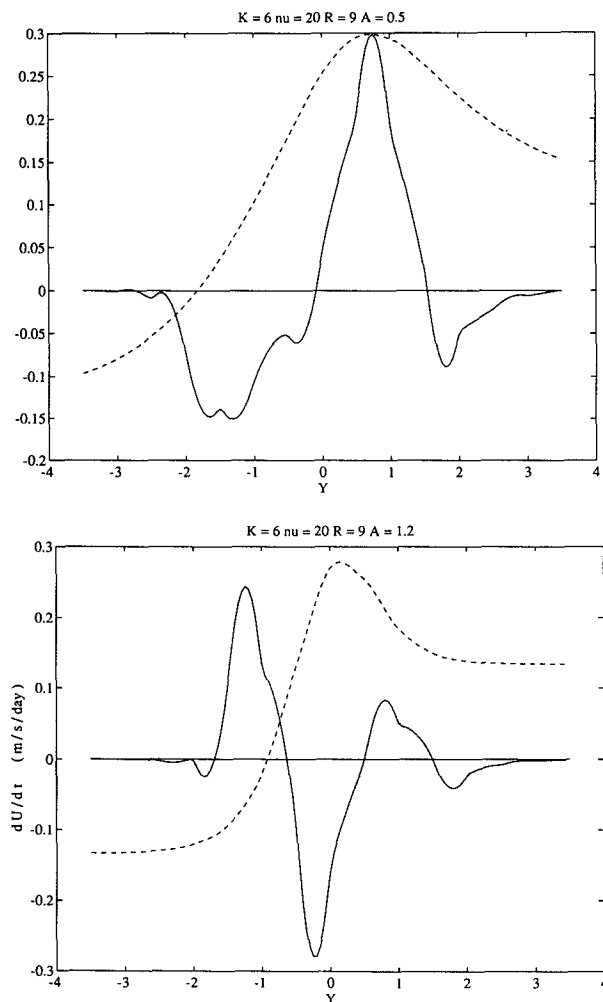

FIG. 21. The vertically averaged eddy momentum flux divergence in m/s/day as a function of latitude. The dissipation parameters are taken to be $\nu = 20 \, m^2 \, s^{-1}$ and $1/R = 9$ days, and the stochastic forcing is $E_{in} = 1 \, W \, m^{-2}$. The dash curve shows the meridional variation of the vertically averaged background flow normalized by the maximum momentum flux divergence: (a) for a jet with width $A = 0.5$ for which there is an upgradient tendency at the jet maximum and simultaneously a tendency for increased asymmetry; (b) for a jet with width $A = 1.2$ for which there is a downgradient tendency at the jet maximum and a tendency for a reduction of the asymmetry. Note that a unit in the abscissa corresponds to approximately 10 degrees of latitude.

than from, for example, a propensity for nonlinear upscale transfer to enhance response at this wavenumber.

Because of the central role of the response of the dynamical operator linearized about the mean flow in this theory, there are some similarities between the stochastic theory and theories envisioning adjustment to neutrality, such as baroclinic adjustment parameterization for heat flux (Stone 1978; Lindzen 1993). In the stochastic theory, however, the instability does not equilibrate the flow because the system is maintained damped by the divergent fluxes resulting as the stability boundary is approached but never reached.

Practically, stochastic dynamics points the way to a consistent parameterization of fluxes associated with equilibrium states that balance the stochastic fluxes with the large-scale thermal forcing. Obtaining this parameterization will be the subject of future work.

REFERENCES

Eliassen, A., 1956: Instability theories of cyclone formation. *Weather Analysis and Forecasting,* Vol. 1, McGraw-Hill.

Farrell, B. F., 1985: Transient growth of damped baroclinic waves. *J. Atmos. Sci.,* **42,** 2718–2727.

——, 1989: Optimal excitation of baroclinic waves. *J. Atmos. Sci.,* **46,** 1193–1206.

——, and P. J. Ioannou, 1993a: Stochastic forcing of perturbation variance in unbounded shear and deformation flows. *J. Atmos. Sci.,* **50,** 200–211.

——, and ——, 1993b: Stochastic forcing of the Navier–Stokes equations. *Phys. Fluids A,* **5,** 2600–2700.

——, and ——, 1993c: Stochastic dynamics of baroclinic waves. *J. Atmos. Sci.,* **50,** 4044–4057.

——, and ——, 1994a: Variance maintained by stochastic forcing of nonnormal dynamical systems associated with linearly stable shear flows. *Phys. Rev. Lett.,* **72,** 1188–1191.

——, and ——, 1994b: A theory for the statistical equilibrium energy and heat flux produced by transient baroclinic waves. *J. Atmos. Sci.,* **51,** 2685–2698.

Fraedrick, K., and H. Böttger, 1978: A wavenumber-frequency analysis of the 500 mb geopotential at 50°N. *J. Atmos. Sci.,* **35,** 745–750.

Gill, A. E., 1982: *Atmosphere–Ocean Dynamics.* Academic Press, 662 pp.

Held, I. M., 1975: Momentum transport by quasi-geostrophic eddies. *J. Atmos. Sci.,* **33,** 1494–1497.

——, 1978: The vertical scale of an unstable baroclinic wave and its importance for eddy heat flux parameterizations. *J. Atmos. Sci.,* **35,** 572–576.

——, and D. G. Andrews, 1983: On the direction of the eddy momentum flux in baroclinic instability. *J. Atmos. Sci.,* **40,** 2220–2231.

Holton, J. R., 1992: *An Introduction to Dynamic Meteorology.* Academic Press, 507 pp.

Ioannou, P. J., 1995: Nonnormality increases variance. *J. Atmos. Sci.,* **52,** 1155–1158.

——, and R. S. Lindzen, 1986: Baroclinic instability in the presence of barotropic jets. *J. Atmos. Sci.,* **43,** 2999–3014.

Joseph, D. D., 1976: *Stability of Fluid Motions I.* Springer-Verlag, 282 pp.

Lesieur, M., 1993: *Turbulence in Fluids.* Kluwer Academic, 412 pp.

Lin, S.-J., and R. T. Pierrehumbert, 1988: Does Ekman friction suppress baroclinic instability? *J. Atmos. Sci.,* **45,** 2920–2933.

Lindzen, R. S., 1993: Baroclinic neutrality and the tropopause. *J. Atmos. Sci.,* **50,** 1148–1151.

McIntyre, M. E., 1970: On the non-separable baroclinic parallel flow instability problem. *J. Fluid Mech.,* **40,** 273–306.

Nordeng, T. E., 1990: A model-based diagnostic study of the development and maintenance mechanism of two polar lows. *Tellus,* **42A,** 92–108.

Palmén, E., and W. C. Newton, 1969: *Atmospheric Circulation Systems.* Academic Press, 603 pp.

Pedlosky, J., 1987: *Geophysical Fluid Dynamics.* Springer-Verlag, 710 pp.

Petterssen, S., 1955: A general survey of factors influencing development at sea level. *J. Meteor.,* **12,** 36–42.

Randel, W. J., and I. M. Held, 1991: Phase speed spectra of transient eddy fluxes and critical layer absorption. *J. Atmos. Sci.,* **48,** 688–697.

Raude, W. J., and J. L. Stanford, 1985: An observational study of medium-scale wave dynamics in the Southern Hemisphere summer. Part I: Wave structure and energetics. *J. Atmos. Sci.,* **42,** 1172–1188.

Salby, M. L., 1982: A ubiquitous wavenumber-5 anomaly in the Southern Hemisphere during FGGE. *Mon. Wea. Rev.,* **110,** 1712–1720.

Salmon, R., 1980: Baroclinic instability and geostrophic turbulence. *Geophys. Astrophys. Fluid Dyn.,* **15,** 167–211.

Sanders, F., 1986: Explosive cyclogenesis in the west-central North Atlantic Ocean, 1981–84. Part I: Composite structure and mean behavior. *Mon. Wea. Rev.,* **114,** 1781–1794.

Schäfer, J., 1979: A space-time analysis of tropospheric planetary waves in the Northern Hemisphere geopotential height. *J. Atmos. Sci.,* **36,** 1117–1125.

Schubert, S., W. Higgins, C.-K. Park, S. Moorthi, and M. Suarez, 1990: An atlas of ECMWF analyses (1980–87). Part II: Second moment quantities. NASA TM 100762, 286 pp.

Stone, P. H., 1978: Baroclinic adjustment. *J. Atmos. Sci.,* **35,** 561–571.

——, S. J. Ghan, D. Spiegel, and S. Rambaldi, 1982: Short-term fluctuations in the eddy heat flux and baroclinic stability of the atmosphere. *J. Atmos. Sci.,* **39,** 1734–1746.

Trenberth, K. E., 1992: Global analyses from ECMWF and atlas of 1000 to 10 mb circulation statistics. NCAR/TN-373, 191 pp.

Vallis, G. K., 1988: Numerical studies of eddy transport properties in eddy resolving and parametrized models. *Quart. J. Roy. Meteor. Soc.,* **114,** 183–224.

Wang, M. C., and G. E. Uhlenbeck, 1945: On the theory of the Brownian motion II. *Rev. Mod. Phys.,* **17,** 323–342.